Water vapor barrier properties of wheat gluten/silica hybrid coatings on paperboard for food packaging applications

Cesare Rovera,[a] Hasan Türe,[b] Mikael S. Hedenqvist,[c] Stefano Farris,[a,*]

[a] DeFENS, Department of Food, Environmental and Nutritional Sciences, University of Milan, via Celoria 2 – I-20133 Milan, Italy

[b] Fatsa Faculty of Marine Science, Department of Marine Science and Technology Engineering, Ordu University, Ordu, Turkey

[c] Department of Fibre and Polymer Technology, School of Engineering Sciences in Chemistry, Biotechnology and Health, KTH Royal Institute of Technology, Stockholm, 10044, Sweden

_____

*Corresponding author

Tel.: +39 0250316805; Fax: +39 0250316672

Email address: stefano.farris@unimi.it (S. Farris)

Abstract

Motivated by the increasing need for new solutions with less environmental impact, in this work we have investigated the benefits of depositing a wheat gluten (WG) coating on paperboard substrates intended for food packaging applications. To overcome the inherent moisture sensitivity of this protein, WG was combined with a silica network obtained by sol-gel chemistry. WG/silica hybrid coatings were characterized in terms of structural, thermal, morphological, surface, and water vapor barrier properties. Spectrometric analysis demonstrated that the organic and inorganic phases interacted primarily through hydrogen bonding. This was also supported by thermal experiments, which revealed a higher T_g measured for the hybrid materials with the higher silica content (114 ± 1 °C and 128 ± 2 °C, respectively) compared to the pure WG material ($T_g = 89 \pm 1$ °C). Scanning electron microscopy showed that the surfaces of the coatings were very smooth, though the presence of pinholes, cracks, fractures, and voids was detected, especially for the silica-rich formulations. Upon deposition of the coatings, the wettability of the bare paperboard increased, as demonstrated by the lower water contact angle values. In addition, hybrid coatings exhibited a higher wettability over the pristine WG coating, which was due to a more intense spreading phenomenon. The deposition of the coatings led to a ~ 4-fold reduction in water vapor transmission rate (WVTR ~ 90 g m^{-2} 24h^{-1} at 23°C and 65% relative humidity) of the specific cellulosic substrate tested in this work (WVTR ~ 350 g m^{-2} 24^{-1}).

1. Introduction

The increased attention to environmental concerns has recently prompted a renewed interest in cellulosic materials, including paper and paperboard, which have been used in numerous applications for centuries. Over time, the use of cellulosic materials has spread, and today, these materials are used by a wide range of industries. In the packaging industry, one of the most economically important applications of cellulosic materials is in the food sector. Paper and paperboard encompass 31% of the global packaging market and are mainly used in food packaging for containment and protection of the food products, convenience during storage or consumption, and communication of the relevant information to consumers, including marketing aspects (Jones & Comfort, 2017). Widespread uses of paper and paperboard concern ice-cream cups, microwave popcorn bags, baking paper, fast food containers such as pizza, beverage cups etc. (Deshwal, Panjagari, & Alam, 2019). In these cases, the main goal of the packaging material is to act as a container, enabling some specific actions such as cooking, handling, and easy consumption of the food. In other applications as primary packaging (i.e., in direct contact with food), paper is a component of a packaging configuration specifically designed to protect the food and extend its shelf life. This is the case, for example, of dry biscuits, milk cartons, chips, juices, fruit, vegetables, bread etc. However, in all the above applications the paper layer is coupled with other layers (most often plastic layers) mainly because paper alone is very high sensitivity to gases (e.g. oxygen and carbon dioxide) and vapors (e.g. water vapor and aromas), which diffuse through the highly porous material (Krook & Hedenqvist, 2002).

Many efforts have been made to address this issue over the years, especially via physical and chemical methods, in an attempt of increasing the utility of cellulosic materials for a wider range of applications. For example, cellulosic substrates have been coupled to various non-cellulosic materials, such as: plastic polymers (e.g. polyethylene – PE and polyethylene terephthalate – PET); natural waxes; and aluminum foil (Deshwal et al., 2019; Mir, Wani, Wani, Singh, & Wani, 2017). Today, these coupling procedures are usually performed by co-extrusion or lamination to obtain multi-layer cellulosic-based materials with barrier properties against water vapor, grease, and oxygen,

making them suitable for most packaging applications (Sun, Schork, & Deng, 2007). However, lamination of paperboard with plastics or aluminum foil decreases the recyclability of the final product.

The ability to improve the overall properties of cellulosic substrates through biopolymer materials is becoming increasingly important for both the scientific and industrial communities, enabling these materials to serve as attractive alternatives to polymers of fossil origin. In particular, improving the barrier properties of cellulosic materials, without jeopardizing their inherent degradability, remains a major challenge. To this end, several solutions have been tested, such as polycaprolactone – PCL (Bota, Krehula, Katančić, Brozovića, & Hrnjak-Murgić, 2017), polylactic acid – PLA (Rhim, Lee, & Hong, 2007), and many natural hydrocolloids in the form of aqueous dispersion coatings including starch, cellulose derivatives, chitosan, alginate, whey proteins, caseinates, zein, soy protein, and wheat gluten (Menzel & Koch, 2014; Andersson, 2009; Ottesen et al., 2017; Gällstedt, Brottman, & Hedenqvist, 2005; Zhang, Xiao, & Qian, 2014; Mazhari Mousavi, Afra, Tajvidi, Bousfiled, & Dehghani-Firouzabadi, 2017; Gatto, Ochi, Pedroso Yoshida, & Ferreira da Silva, 2019; Mirmehdi, Gherardi Hein, Grígoli de Luca Sarantópoulos, Dias, & Denzin Tonoli, 2018).

Among biopolymers, the interest towards wheat gluten (WG) lies in its functional properties, wide availability and low cost since it is a by-product of starch production for e.g. ethanol biofuel (Lens et al., 2003; Farrell et al., 2006). In addition, WG displays suitable material properties as well as good biodegradability (Sartori, Feltre, do Amaral Sobral, Lopes da Cunha, & Menegalli, 2018). Besides the above-mentioned advantages, the long-lasting interest in WG for food packaging applications is mainly due to its good barrier properties against gases (e.g., oxygen and carbon dioxide) in dry conditions, which make WG a viable solution to control the inherent permeability to gas of cellulosic materials (Hedenqvist, 2018; Guillaume, Pinte, Gontard, & Gastaldi, 2010; Olabarrieta et al., 2006; Gontard, Guilbert, & Cuq, 1992; Gontard, Guilbert, & Cuq, 1996; Mujica Paz & Gontard, 1997; Mujica Paz, Guillard, Reynes, & Gontard, 2005). However, a drawback is the

high sensitivity to moisture, which causes a marked decrease of the gas barrier properties at high

relative humidity, restricting its potential use to breathable foods, such as fruit and vegetables. This

is why, for example, gluten films/coatings tend to swell when in contact with aqueous media. For the

same reason, the water vapor permeability values for WG films were reported to be 2-5 orders of

magnitude greater than those of typical polymeric packaging films, such as polypropylene (PP),

polyethylene (PE), polyvinylidene chloride (PVC), and polyethylene terephthalate (PET) (Gennadios,

Brandenburg, Park, Weller, & Testin, 1994). As widely reported in the literature, this is primarily due

to the inherent hydrophilic nature of the WG protein as well as to the substantial amount of

hydrophilic plasticizer (e.g. glycerol) generally added to impart adequate film flexibility (Tunc et al.,

2007).

To date, many different approaches have been used to address the water sensitivity of WG

materials, including coating a thin layer of polyethylene terephthalate, thermal treatment-mediated

polymer network modifications, the use of mixed WG and hydrophobic biodegradable polymers (e.g.

polycaprolactone), mixing WG with polysaccharides to yield structural complexes, or incorporation

of nanofillers such as montmorillonite (Sartori et al., 2018; Mascheroni, Guillard, Gastaldi, Gontard,

& Chalier, 2011; Das et al., 2020; Türe, Gällstedt, Johansson, & Hedenqvist, 2013). In the present

study, we propose an alternative approach to improve the water vapor barrier properties of

paperboard, based on the development of WG-based hybrid coatings through sol-gel chemistry. This

approach is widely adopted in the coating technology because of its versatility, low cost, and low

environmental impact, especially compared to hard-chemistry synthesis routes (Rovera, Ghaani, &

Farris, 2020). For example, hybrid coatings were obtained by sol-gel chemistry to improve the oxygen

barrier properties of plastic films (Farris et al., 2012; Fuentes-Alventosa et al., 2013; Startek,

Marczak, & Lukowiak, 2020). Sol-gel hybrid coatings were also prepared to obtain antimicrobial

(Corradini et al., 2013; Lantano et al., 2014; Razavi, Tajik, Moradi, Molaei, & Ezati, 2020),

antioxidant (Bossi, Tana, Punta, Cigada, & De Nardo, 2016) and intelligent (Liu et al., 2020) food

packaging materials. In these previous works, the inorganic phase (silica-based) was used in

combination with an organic counterpart represented by a biopolymer, such as pullulan, chitosan, poly-lysine, etc. However, to our knowledge, the use of the sol-gel technology to improve the water vapor barrier performance of WG coatings on cellulosic substrates intended for food packaging applications has never been reported before.

2. Fundamental chemistry underlying development of WG-silica hybrid materials

The use of the sol-gel approach is widely used in the coating technology to obtain hybrid materials with high performance, in spite of the reduced thickness of the final layer (from tenths of nm up to few microns) (Rovera, Ghaani, & Farris, 2020). More recently, the sol-gel technology has been extended for the generation of hybrid coatings obtained from metal alkoxides (e.g., tetraethoxysilane, TEOS) in combination with biopolymers (Razavi et al., 2020). The overall process accounts for two main steps, i.e. hydrolysis and condensation (Figure 1). Hydrolysis occurs by the nucleophilic attack of the oxygen contained in water on the silicon atom, according to the reaction scheme reported in Figure 1a. However, protonation of alkoxide groups is faster if an acid is used as a catalyst, although the base-catalyzed hydrolysis is also well established (Schubert, 2015). Alkoxide groups (–OR) of the precursor are then replaced with hydroxyl groups (-OH) to form the silanol compounds $-Si(OH)_n$, whereas ethanol is the by-product.

Upon hydrolysis and in presence of the organic phase, two main different pathways can possibly involve the silanol groups. On one hand, $Si(OH)_n$ may react according to a typical condensation scheme by two different routes (water condensation and alcohol condensation) to yield in both cases SiO_2 covalent bonds and water or alcohol as by-products (Figure 1b). On the other hand, the $Si(OH)_n$ groups can interact by secondary forces (e.g., hydrogen bonds) with the pendant polar group along the backbone of the organic polymer (Farris et al., 2012). In this work, we assumed that hydrogen bonding can occur between the polar groups of most abundant wheat gluten amino acids (e.g. –OH and $-NH_2$ groups of glutamic acid, aspartic acid, serine, threonine, asparagine, arginine, lysine) and the silanol groups, which will simultaneously form the glass-like oxidic network by new SiO_2

131 covalent bonds (Figure 1c). Eventually, both the *in-situ* synthesis of SiO_2 in the WG water dispersions

132 and the hydrogen bonds formation can explain the overall performance that is expected in the final

133 hybrid materials.

134

135 **3. Materials and Methods**

136 *3.1 Reagents and chemicals*

137   Commercial wheat gluten powder was kindly supplied by Lantmännen Repper AB, Sweden.

138 According to the supplier, the gluten protein content was 77.7 wt% (dry basis) (modified NMKL Nr

139 6, Kjeltec, Nx5.7, www.NMKL.org), the moisture content was 6.9 wt% of the total weight (NMKL

140 23, 1991), and the starch content was 5.8 wt% (dry basis) (Ewers, polarimetric method). The

141 concentration of fats was 1.2 wt% (dry basis) (Soxtec, Lidfett.OA.19, tecator AN 301), and the ash

142 content was 0.9 wt% (dry basis) (NMKL 173 2nd ed). High purity TEOS (Sigma-Aldrich, Stockholm,

143 Sweden) was used as a metal alkoxide precursor of the inorganic phase; 1 M hydrochloric acid

144 (Sigma-Aldrich, Stockholm, Sweden) was used as a catalyst. Pure acetic acid and sodium sulphite

145 (Sigma-Aldrich, Stockholm, Sweden) were used to prepare the wheat gluten dispersions. Paperboard

146 samples (Korsnäs Duplex 260) were provided by Korsnäs AB, Gävle, Sweden. The bottom layer of

147 the paperboard, which was used as a substrate for the coatings, consisted of unbleached softwood

148 sulphite pulp, while the middle layer consisted of unbleached chemithermomechanical pulp (CTMP).

149 The top hydrophobic layer consisted of a blend of bleached softwood and hardwood, which was

150 treated using a dual glue, containing alkyl ketene dimer (AKD) and resin glue. The thickness of the

151 paperboard samples ranged between 350 μm and 400 μm. Ethanol (Sigma-Aldrich, Milan, Italy) and

152 Milli-Q water (18.3 MΩ · cm) were used for the hybrid coating dispersion preparations. All materials

153 were used as received.

154

155 *3.2 Preparation of hybrid coatings*

156   Hybrid coatings were prepared according with the procedure proposed by Türe et al., with slight

157   modifications (Türe, Blomfeldt, Gällstedt, Hedenqvist, & Farris, 2013). Briefly, an acidic (pH = 2.0

158   ± 0.8) hydro-alcoholic (30 wt% ethanol) solution of TEOS was prepared using 1M HCl (0.78 wt%)

159   as a catalyst, with a fixed H_2O:TEOS molar ratio of 4:1. TEOS hydrolysis was conducted at room

160   temperature for approximately 1 hour. At the same time, an aqueous dispersion of wheat gluten was

161   prepared at room temperature, by mixing gluten powder into water containing sodium sulphite (2.5

162   mg/g wheat gluten) as a reducing agent, for 30 minutes under gentle stirring (500 rpm). Acetic acid

163   was then added to the mixture in order to adjust the pH to 4.0. Air bubbles possibly formed during

164   stirring were removed using a sonicator bath (mod. 2510, Branson, Danbury, USA) at room

165   temperature for 2 minutes. The inorganic and organic phases were then mixed together for 1 hour, to

166   facilitate formation of the hybrid network. To investigate the influence of the organic/inorganic ratio

167   (O/I, defined as the wheat gluten/$(SiOH)_4$ weight ratio for a complete hydrolysis process) on the final

168   water vapor barrier properties of the composites, six different coating dispersions were prepared, by

169   varying the O/I ratio of the coatings from 100/0 to 50/100, as reported in Table 1. Note that subscripts

170   indicate the O/I ratio (for example, H_1 stands for hybrid with O/I = 1). The composite solutions were

171   then deposited onto the paperboard samples using a steel horizontal wire wound rod (S26, RD

172   Specialties Inc, Webster, NY), with a wire diameter of 660 μm, enabling deposition of a wet thickness

173   of 59 μm (i.e. a dry thickness of approximately 12 μm for a water-based 20 wt% dispersion, assuming

174   a density equal 1 g cm^{-3}). Coated paperboard samples were dried first by using a constant and

175   perpendicular flux of mild air (25.0 °C ± 0.3°C) at a distance of 40 cm from the applicator for 2 min.

176   In the second step, composite films were stored in an oven at 40°C for 24 hours.

177

178   *3.3 Fourier Transform Infrared – Attenuated Total Reflectance (FTIR- ATR) Analysis*

179   Physicochemical properties of WG coatings at different silica concentrations were investigated

180   using a PerkinElmer FT-IR Spectrum^{TM} 100 Series spectrometer (PerkinElmer, Waltham, MA, USA)

181   equipped with a universal attenuated total reflectance (UATR) accessory with the single-reflection

sampling plate of 1.8 mm round germanium surface. To ensure satisfactory physical contact between samples and crystal surface, a high-pressure clamping device was used. Spectra were recorded at room temperature within the range of 600–4000 cm^{-1} at 4 cm^{-1} resolution. Spectrum 6.0 software was used for data acquisition and analysis.

3.4 Thermal properties

The thermal properties of both WG and hybrid film samples were determined by differential scanning calorimetry (DSC) analysis using a DSC 1 (Mettler Toledo, Columbus, OH) supplied with a quench-cooling accessory and a GC 100 gas controller. Before measurements, the instrument was calibrated with the well-characterized standard indium, which has a heat of fusion (ΔH) of 28.4 J/g and a melting temperature (T_m) of 156.6 °C. Approximately 5 mg of WG or WG/silica samples were then put in aluminum pans (40 μL) which was hermetically sealed and holed to allow the entrance of the purge gas. All the thermograms were obtained in an inert environment (50 mL min^{-1} N$_2$) at a rate of 10 °C min^{-1}. An initial scan from -50 to 300 °C was followed by an isothermal step (300 °C for 5 min), with the goal of removing the residual moisture. Samples were then cooled down to -50°C to erase the thermal history. A second heating scan was finally carried out from -50 to 300 °C for the determination of the glass transition temperature (T_g). For the determination of the specific heat capacity (c_p) of pure WG and hybrid materials, the same protocol as above was used, with the exception of the final temperature of the heating cycle, which was set at 180°C to avoid any possible influence on the c_p due to thermal degradation of the matrix.

3.5 Field-Emission Scanning Electron Microscopy (FE-SEM)

Both the coated surfaces and cross-sections of the films were examined using a Hitachi S-4800 FE-SEM. Samples were dried in a desiccator in the presence of silica gel for a minimum of 48h before examination. Surface test specimens were mounted with carbon tape on stubs. Cross-sectioned samples were cut into thin pieces with a scalpel, and mounted on a Hitachi thin specimen split mount

208 holder, M4 (prod. No 15335-4), to observe the cross-section and determine the thickness of the

209 coating. Before insertion in the microscope, samples were coated with gold to a thickness of ca. 10

210 nm (to avoid charging the samples), using an Agar High Resolution Sputter Coater (model 208RH),

211 equipped with a gold target/Agar thickness monitor controller.

212

213 *3.6 Optical Contact Angle (OCA)*

214 The wettability of the coated surfaces was assessed using an optical contact angle apparatus

215 (KSV CAM 200, Espoo, Finland), equipped with a Basler A602f camera. The contact angle of water

216 in air was measured on rectangular (5×2 cm^2) coated paperboard samples by the sessile drop method.

217 This method consists of gently dropping a droplet of 4 ± 0.5 µL of Milli-Q water (18.3 MΩ·cm) onto

218 the coated surface, according to the so-called pick-up procedure. Specifically, a droplet hanging on

219 the end of a needle is laid on the coating surface by raising the sample stage until solid/liquid contact

220 is made. Analyses were conducted in a climate-controlled room (23 °C and 50 % relative humidity

221 (RH)). All droplets were released from a height of 1 cm above the surface, to ensure consistency

222 between each measurement. The evolution of the contact angle (θ, the angle between the baseline of

223 the drop and the tangent at the drop boundary), the droplet volume (V, µL) and the droplet surface

224 area (A, mm^2), were monitored using a software-assisted image processing procedure, which fits the

225 drop profile with the Young-Laplace equation. The values of these parameters were collected 2 times

226 per second during the first 10 seconds and 1 time per second during the following 50 seconds of

227 analysis, starting from the deposition of the drop ($t_0 = 0$ s) to 60 s ($t_{60} = 60$ s). A minimum of 10

228 droplets were examined for each sample on both the left and right sides, and resulting mean θ values

229 were then used for the calculations described below.

230

231 *3.7 Water vapor barrier properties*

232 Water vapor transmission rates (WVTR) of both uncoated and coated paperboard samples were

233 assessed using a Multiperm permeability analyzer (ExtraSolution® Srl, Capannori, Italy) equipped

234   with an infrared sensor and based on the isostatic method. Specimens were sandwiched between two

235   aluminum-tape masks, allowing a surface of 2.01 cm^2 to be exposed to the permeation of water vapor.

236   WVTR values (g m^{-2} 24 h^{-1}) were determined using the standard method ASTM F1249, with a carrier

237   flow (N_2) of 10 mL min^{-1}. Measurements were performed at 23°C and 65 % RH, which is the humidity

238   gradient between the two semi-chambers between which the sample was mounted. Each WVTR value

239   was from five replicates.

240

241   *3.8 Statistical analysis*

242   Data were analyzed using Statgraphics Plus 4.0 software (STSC, Rockville, MD, USA), and

243   one-way analysis of variance was used to check for differences between samples. The significance

244   level (*p*) was fixed at 0.05.

245

246   **4. Results and Discussion**

247   *4.1 Thickness of the composites*

248   SEM micrographs (Figure 2) revealed that all samples were slightly thinner than theoretically

249   predicted, with an average value of 9.5 ± 1.5 μm, rather than ~ 12 μm (assuming a 20 wt% dry matter

250   content in the dispersion). The variability was quite high (relative standard deviation ~ 30%) within

251   samples (i.e., for a same sample), which may be due to the highly heterogeneous surface of the

252   paperboard and to an uneven distribution of the coating throughout the fibrous surface. In addition,

253   the difference between theoretical and measured thickness values appears to be more pronounced

254   with increasing O/I ratio, which was probably due to the increasing amount of ethanol as a by-product

255   of the condensation step of the sol-gel reaction. However, no statistically significant difference was

256   observed between samples. We also determined the grammage of the coating (coating weight per unit

257   surface, g/m^2) gravimetrically, i.e., weighing 1 dm^2 of the cellulosic substrate with and without

258   coating, the difference being then scaled to 1 m^2, according to Gatto et al. (2019). The average

259   grammage of the coatings was 10.5 ± 1.5 g/m^2, with no statistically significant difference among

260   formulations. The final appearance of all composites (i.e. paperboard + coating) indicated a bi-layer

261   structure, with no clear evidence of interpenetration between the two contacting layers.

262

263   *4.2 WG–silica hybrids formation*

264   FT-IR can provide detailed information on the nature of interphase bonding. FT-IR spectra of

265   pure wheat gluten and reacted TEOS (i.e., after hydrolysis and condensation) have been discussed

266   elsewhere (Türe et al., 2013). Figures 3a-c show the three spectral regions that underwent the most

267   significant changes as a function of O/I ratio. Association of the two phases produced dramatic

268   changes in the FT-IR spectra of the resulting hybrid coatings. For clarity, each of the three spectral

269   regions which underwent significant changes is discussed separately below.

270   In the region (3850 cm^{-1} – 2400 cm^{-1}, Figure 3a) decreasing the O/I ratio (i.e., moving from the

271   formulation H_3 to $H_{0.5}$) resulted in a broadening of the band at ~ 3300 cm^{-1} assigned to amide A and

272   B (N-H stretching vibration) of WG. This mode of vibration has been shown to be independent of

273   backbone conformation, but is very sensitive to hydrogen bond strength (Krimm & Bandekar, 1986).

274   Accordingly, peak broadening in this region could possibly be due to extensive hydrogen bonding

275   between silanol and hydroxyl groups of the organic phase (Lee, Lee, & Yang, 1999; Bandyopadhyay,

276   De Sarkar, & Bhowmick, 2005; Tong, Xiao, & Lim, 2008).

277   The second region (1720 – 1470 cm^{-1}, Figure 3b) contains the two major bands of the protein

278   infrared spectrum: amide I (~ 1650 cm^{-1}) and amide II (~ 1530 cm^{-1}), whose peak intensities are

279   directly influenced by the backbone conformation (the secondary structure of the protein). As can be

280   seen in the inset in Figure 3b, even the lowest concentration of silica tested (O/I = 3) produced

281   significant changes in the amide I band, which is intimately related to the physical structure of the

282   wheat gluten chains. More specifically, the bands at 1651 cm^{-1} and 1644 cm^{-1} can be assigned to α-

283   helices/random coils and disordered domains, respectively; while bands at 1635 cm^{-1} and 1625 cm^{-1}

284   are attributed to β-sheet conformations with a high or low level of hydrogen bonding, respectively

285   (Cho, Gällstedt, & Hedenqvist, 2010; Cho, Gällstedt, Johansson, & Hedenqvist, 2011). The addition

286 of the inorganic phase reduced the width of the peak assigned to amide I from 1640 cm^{-1} to 1620 cm^{-}

287 ^{1} (see the inset in Figure 3b). Simultaneously, the peak centered at 1651 cm^{-1} increased considerably

288 in the H$_3$ sample, and even more markedly in the other hybrid coatings, with decreasing O/I ratio.

289 These observations clearly demonstrate that the presence of the inorganic phase has a 'destructuring'

290 effect on the main WG network. More specifically, the presence of silica interferes with the formation

291 of an ordered secondary structure, increasing the proportion of random coil and disordered regions in

292 the WG matrix, confirming our previous findings obtained on WG/silica 3D hybrid materials (Türe

293 et al., 2013).

294   In the third region (1150 cm^{-1} – 700 cm^{-1}, Figure 3c), the band centered at ∼945 cm^{-1}, which

295 was assigned to silanol groups (Si–OH) in the reacted TEOS spectrum, shifted toward higher

296 wavenumbers, especially in the case of the H$_3$ formulation (peak centered at 962 cm^{-1}). In addition,

297 the extent of this shift is gradually reduced as the O/I ratio is decreased; and for sample H$_{0.5}$ no shift

298 was observed. These results are in contrast to those previously reported for pullulan/silica hybrid

299 coatings, where shifting of the same peak toward higher wavenumbers with increasing inorganic

300 phase was attributed to a corresponding increase in hydrogen bonding between the organic and

301 inorganic phases (Farris et al., 2012). Interestingly, the peak assigned to silicon oxide (SiO$_2$)

302 asymmetric stretching (∼1060 cm^{-1}) shifted to a slightly higher wavenumber (1064 cm^{-1}) at the lowest

303 silica concentration; while a shift toward lower wavenumbers was observed as the O/I ratio decreased,

304 up to 1040 cm^{-1} for the sample H$_{0.5}$. Therefore, it is likely that other forces in addition to hydrogen

305 bonding are responsible for driving the interactions between the two phases (organic and inorganic);

306 because, although O/I < 3 was mostly driven by hydrogen bonding, decreasing the O/I ratio promoted

307 different interactions involving the SiO$_2$ network. This hypothesis seems to be supported by the

308 disappearance of peaks centered at 1730 cm^{-1} and 1233 cm^{-1}in the pure WG spectrum, which might

309 reflect either the establishment of new bonds involving carbonyl groups along the WG backbone, or

310 interaction of the silica with WG reactive groups (e.g. –OH groups) to form Si-O-C bonds, as already

311 postulated for polyvinyl alcohol/silica hybrids (Uragami, Okazaki, Matsugi, & Miyata, 2002; Minelli,

13

312   De Angelis, Doghieri, Rocchetti, & Montenero, 2010). However, whether these new bonds in the

313   hybrid coatings can be considered to be covalent in nature is still under investigation.

314

315   *4.3 Differential Scanning Calorimetry*

316   DSC analyses were performed with the goal of corroborating the information obtained from the

317   FT-IR test concerning the structural changes in the WG network upon interaction with the inorganic

318   phase. Figure 4 displays the DSC traces of pure WG samples and of the hybrid materials containing

319   an equal amount (H_1) and twice the amount of ($H_{0.5}$) of silica compared to that of WG. In the first

320   heating scan (Figure 4a) a main endothermal region above 200 °C can be observed for the three

321   samples, with a sharp peak centered at 216 ± 1 °C, 239 ± 2 °C, and 271 ± 2 °C for the samples H_0,

322   H_1 and $H_{0.5}$, respectively. The shift of the endothermal peak to higher temperatures moving from the

323   formulation H_0 to the formulation $H_{0.5}$ is a clear evidence of the protective role of silica in terms of

324   thermal stability of the WG network, confirming what was observed for WG-silica biofoams (Wu et

325   al., 2014). Samples H_0 and H_1 also showed a second endothermal peak (at 264 ± 1 °C and 256 ± 2

326   °C, respectively) (Figure 4a), which was not detected in sample $H_{0.5}$, probably because of the

327   protective role of silica. These endothermic peaks at relatively high temperatures can be attributed to

328   the thermal degradation of the main polymer phase, with special reference to the functionalities of

329   the protein primary structure. This is in agreement with previous TGA experiments, which showed

330   the degradation of the pure WG sample occurred in two main temperature regions, whereas in the

331   hybrid composites most weight loss occurred in only one step (Türe et al., 2013).

332   The second heating scan (Figure 4b) revealed differences in the second order transition

333   experienced by the samples. The higher T_g measured for the hybrid materials H_1 and $H_{0.5}$ (114 ± 1 °C

334   and 128 ± 2 °C, respectively) compared to the pure WG material H_0 (T_g = 89 ± 1 °C) can be explained

335   as a consequence of the new interactions (hydrogen bonds) between the two phases, hence confirming

336   what the findings arising from the FT-IR analyses. These new bonds would have eventually restricted

337   the segmental mobility of the molecular chains within the amorphous regions, thus increasing the

338   glass transition temperature.

339   A quantitative determination of the specific heat capacity (c_p) of the different materials was

340   possible considering the inflexion in the base line of DSC thermograms obtained from -50 °C to 180

341   °C, and using the general equation for the total heat flow at any point in a DSC experiment given by

342   (Hatakeyama & Quinn, 1999):

$$\frac{\partial Q}{\partial t} = C\ \beta + f(T,t) \tag{1}$$

344   where: $\partial Q/\partial t$ (J min^{-1}) is the heat flow, that is, the amount of heat transferred per unit time; C (J K^{-1})

345   is the sample heat capacity; β (K min^{-1}) is the constant heating rate; $f(T, t)$ is the heat flow associated

346   to the kinetic processes that are (absolute) temperature and time dependent. The heat capacity

347   component of the total heat flow, $C\ \beta$, is generally referred to as the reversing heat flow, while the

348   kinetic component, $f(T, t)$, being referred to as the non-reversing heat flow. Therefore, the specific

349   heat capacity (c_p) profile in the second order transition region (i.e. where the kinetic component can

350   be assumed to be equal to zero) can be obtained according to the following expression:

$$c_p = \frac{\partial Q}{\partial t} \cdot \frac{1}{\beta m} \tag{2}$$

352   following the three-steps procedure proposed by Coleman and co-workers (Coleman & Craig, 1996).

353   c_p is the specific heat capacity in J g^{-1} K^{-1} and m is the mass of the sample in g. The knowledge of

354   the specific heat capacity variation at T_g is of great importance especially in an attempt of determining

355   the T_g of materials obtained by two (or more) miscible polymers through the Couchman–Karasz

356   thermodynamic model (Couchman & Karasz, 1978). As can be seen from Figure 5, the c_p at T_g

357   associated to the baseline displacement in the 'reversing' heat flow signal for the materials made of

358   only WG was of 0.11 J g^{-1} K^{-1}, i.e. of the same order of magnitude as the previously determined value

359   of wheat gluten (0.22 J g^{-1} K^{-1}) (Kalichevsky, Jaroskiewicz, & Blanshard, 1992) and of the glutelin

360   fraction of corn gluten (0.184 J g^{-1} K^{-1}) (Di Gioia, Cuq, & Guilbert, 1999). The c_p values calculated

361   for the hybrid materials H_1 and $H_{0.5}$ were instead 0.104 J g^{-1} K^{-1} and 0.081 J g^{-1} K^{-1}, respectively,

362   which can be ascribed to the protective (insulating) role of silica.

363

364   *4.4 Microstructural observations*

365   SEM was used to analyze the structure and morphology of both uncoated and coated samples,

366   as shown in Figure 6. The surface of the uncoated paperboard shows a network of fibers of different

367   sizes stuck, which however does not prevent the occurrence of pinholes (Figure 6a). The deposition

368   of the WG coating provided adequate coverage of the pristine surface. Decreasing the O/I ratio in the

369   coating formulations (that is, moving from the formulation H_3 to the formulation $H_{0.5}$) apparently led

370   to a less coverage of the cellulosic surface (Figures 6c–e), which may be due to the increased ethanol

371   (a by-product of the hydrolysis and condensation reactions of TEOS) in formulations with a higher

372   content of the inorganic phase. It is plausible that both the increased amount of ethanol and the

373   increasing amount of TEOS with decreasing the O/I ratio of the coating formulations, have

374   concurrently contributed a slight penetration of the WG-based dispersion into the network of

375   cellulosic fibers, due to changes in the rheological properties.

376   Noteworthy, all hybrid coatings exhibited cracks and fractures (Figure 6f), and this trend

377   became more obvious as the O/I ratio decreased, due to the inherent rigidity of the silica network. In

378   agreement with previous works, these ruptures may be caused by mechanical stress, triggered by

379   shrinking of the matrix during the solvent evaporation (Lee et al., 1999; Kim, 2008; Fabbri et al.,

380   2006). In general, the coatings had a very smooth surface, with small crater-like dimples evenly

381   distributed over the observed area (see the inset in Figure 6f), which is linked to the large number of

382   pores across the coating thickness, probably arising from air bubbles that remained trapped in the

383   hybrid dispersion in spite of the sonication treatment performed after the coating solution preparation.

384

385   *4.5 Wettability of paperboard-coated surfaces*

386   The wettability of both neat and coated paperboard surfaces was assessed by monitoring the

387   water droplet evolution (expressed in terms of θ, ΔV and ΔA) over 60 s, which was previously shown

to be the time span where most of the total variation occurs in biopolymer coatings (Farris et al., 2011). In preliminary experiments, the contribution of evaporation phenomenon to the variation in total contact angle was quantified according to the method of Karbowiak and co-workers (Karbowiak, Debeaufort & Voilley, 2006) by directly measuring the contact angle on a Teflon® substrate, under the assumption that neither absorption nor spreading occurs over the 60 s interval (thus, any possible variation in θ must be due to evaporation). As can be seen in Table 2 and Figure S1, the variation in contact angle due to evaporation was approximately 2°, corresponding to droplet volume (ΔV) and surface area (ΔA) reductions of 4.5 ± 0.8 % and 3 ± 0.5 %, respectively.

The uncoated paperboard surface exhibited a fairly high initial contact angle ($\theta_0 \sim 125°$), well above 90°, which is often reported as the boundary between hydrophilic ($< 90°$) and hydrophobic surfaces ($\geq 90°$) (Lein, 2019). This can be explained by a double effect. On the one hand, according to the Wenzel's and Cassie-Bexter's theories, effects due to the presence of rough surface topography can be ruled out (Rosario et al., 2004; Wu, Zheng, & Wu, 2005). On the other hand, it is likely that the alkyl ketene dimer-based glue used in the paper manufacturing made the cellulose fibers more hydrophobic. The initial contact angle did not change significantly throughout the 60 s span, indicating that neither absorption nor spreading took place (Farris et al., 2011). In agreement with this, the evolution of both droplet volume and surface area were within the experimental evaporation range (see Figure S2).

Deposition of pristine WG coating dramatically changed the wettability features of the paperboard substrate. Compared to the uncoated paper, θ_0 decreased to $\sim 71°$ (see Table 2), consistent with the more hydrophilic nature of the protein biopolymer, and the fact that deposition of the WG gluten enabled nearly complete coverage of the cellulosic fibers (see Figure 6b). After 60 s, the contact angle decreased by approximately 10° due to both spreading ($\Delta A \sim 2\%$) and absorption ($\Delta V \sim -5\%$) of the water droplet (see Figure S2).

17

412   Addition of a small amount of silica (H$_3$) to the original WG-based coating formulation induced

413   important changes in the sample, especially with respect to the water contact angle evolution. In

414   particular, an additional decrease in θ (~ 20°) was observed as soon as the drop was placed on top of

415   the coating (Figure S3), because of intense spreading over the first 7 s of analysis. More specifically,

416   the surface area of the water droplet increased by ~ 12% during this narrow time interval, but then

417   remained rather stable for the rest of the analysis (Figure S2). The total volume variation (ΔV)

418   accounted for ~ -5%, indicating that absorption across the composite thickness was limited.

419   Therefore, in line with the very high surface energy of glass and ceramics (~ 170 mJ m^{-2}), addition of

420   a small amount of silica made the composites more wettable, while conferring resistance to water

421   absorption during the 60 s evolution experiment.

422   Increasing the silica content did not result in any significant changes in θ_0 (Table 2), with a

423   mean θ_0 value of 77° for all hybrid coatings (with the only exception of sample H$_1$). This unexpected

424   behavior can be plausibly explained taking into account two opposite and counterbalancing effects:

425   i) an increased silica content would increase the polar component of the surface free energy, thus

426   lowering the initial contact angle; ii) increasing the silica content yielded a less coverage of the

427   underlying cellulosic surface (as shown by the SEM analyses). Thus, it is likely that the hydrophobic

428   properties associated with the paperboard fibers would counteract the hydrophilic properties imparted

429   by the silica network. The same coating formulations exhibited similar final contact angle values (θ_{60};

430   around 67°) (Table 2) and a similar size in droplet volume variations (between -4 % and -6 %; see

431   Figure S2), confirming the rather moderate absorption phenomenon.

432

433   *4.6 Barrier properties*

434   Permeation of water molecules across cellulosic materials is one of the major drawbacks of

435   these substrates, severely limiting their use in numerous applications. Biopolymer coatings can be

436   used in reducing this permeability, thus enabling new uses for cellulosic materials without

437   compromising the overall biodegradability of the final material. As shown in Figure 7, a clear

438 decrease of WVTR was observed after coating deposition (both WG and WG-silica hybrid coatings

439 led to a WVTR reduction of ~ 37% for WG and between 63% and 74% for the hybrid coatings).

440 Apparently, the best performance was obtained with the highest O/I ratio, that is, for the coating

441 formulation containing the lowest amount of silica. As the amount of silica increased, the positive

442 effect of the inorganic phase was overshadowed by the intensive cracking. The differences in WVTR

443 between the formulations can also be explained by considering the morphology of the coatings, as

444 displayed in Figure 6. With increasing silica content, a less effective coverage of the original fibrous

445 surface was observed. Consistent with this, it is likely that the number of voids/pores and pinholes

446 also increased, resulting in higher WVTR values. However, the result may also have been affected

447 by differences in the intrinsic heterogeneity of the cellulosic substrate, and thus local differences in

448 the final thickness of the whole composite (paperboard plus coating) within the same sample. Due to

449 these considerations, in can be said that the WVTR results must be taken with care because several

450 factors made an absolute interpretation difficult. For this reason, addressing the above issues

451 (cracking of the coating due to internal stresses, uneven coverage of the cellulosic substrate, and

452 penetration of coating into the fibrous network) is of utmost importance to obtain the actual barrier

453 performance of the coatings. At the same time, if we consider that the above limitations could be

454 addressed, the WVTR values obtained in this work are somehow encouraging, especially if compared

455 to previous information. As reported in Table 3, our results are in line with those obtained using

456 cellulose nanofibers (CNFs) blended with carboxy methyl cellulose (CMC) (Mazhari et al., 2017)

457 and polycaprolactone (PCL) (Bota et al., 2017), while being superior than those reported for zein

458 coatings (Parris, Dickey, Wiles, Moreau, & Cooke, 2000).

459 However, none of the several coating solutions tested on paper/paperboard substrates led to a

460 reduction of WVTR to values that can be deemed suitable for most food packaging applications

461 (below ~ 5 g/m^2 24h), confirming that a high water vapor barrier biopolymer coating for a cellulosic

462 substrate still remains a challenge.

463

4.7 Safety considerations

While the functional properties of a packaging material are often regarded as the first goal to achieve, safety aspects related to food contact materials should be considered with special attention from the first steps of the design of a new packaging solution. In this study, we developed deliberately a hybrid coating by a sol-gel approach (rather than using nanoparticles, e.g., nanoclays, graphene, nanocellulose, etc.) keeping in mind that nanostructured coatings obtained by a bottom-up approach (e.g., sol-gel chemistry) do not fall into the category of nanomaterials as defined in EU Recommendation 696/2011, because they do not consist of primary particles with defined physical boundaries (Störmer, Bott, Kemmer, & Franz, 2017). It is thus reasonable to think that nanostructured materials for food contact applications can be used as long as the chemicals used to form or modify the network are authorized according to EU Regulation n. 10/2011 (Rovera, Ghaani, & Farris, 2020).

5. Conclusions

In this study, we evaluated the possibility of using the sol-gel method to obtain hybrid coatings based on wheat gluten and silica to improve the water vapor resistance of wheat gluten coatings on a cellulosic substrate. In spite of the high potential of this approach to yield high-performance coatings, the experimental results highlighted some limitations of the resulting structures that hinder any possible application. In particular, the inherent rigidity of the inorganic phase led to a high degree of brittleness, to the disadvantage of the final water vapor barrier performance of the hybrid coatings. To overcome this drawback, next steps can include either the use of plasticizers or the selection of network-modifier precursors, possibly with medium-to-long aliphatic tails that would make the hybrid networks less rigid. Finally, other important functional properties (e.g., the permeability to gases, printability, sealability, and flex crack resistance) should be evaluated before market applications.

490   **References**

491   Andersson, C. (2009). New ways to enhance the functionality of paperboard by surface treatment – a

492   review. *Packaging Technology and Science*, *21*, 339–373. https://doi.org/10.1002/pts.823.

493   Bandyopadhyay, A., De Sarkar, M., & Bhowmick, A. (2005). Poly(vinyl alcohol)/silica hybrid

494   nanocomposites by sol-gel technique: synthesis and properties. *Journal of Materials Science*, *40*,

495   5233–5241. https://doi.org/10.1007/s10853-005-4417-y.

496   Bossi, E., Tana, F., Punta, C., Cigada, A., & De Nardo, L. 2016. Flexible hybrid coatings with

497   efficient antioxidation properties. *Food Packaging and Shelf Life*, *10*, 106–114.

498   https://doi.org/10.1016/j.fpsl.2016.10.002.

499   Bota, J., Kratofil K., L., Katančić, Z., Brozović, M., & Hrnjak-Murgić, Z.(2017).   Surface

500   characteristics and enhancement of water vapour properties of paperboard coated with

501   polycaprolactone nanocomposites. *Journal of Adhesion Science and Technology*, *31*, 466–486.

502   https://doi.org/10.1080/01694243.2016.1218313.

503   Cho, S. W., Gällstedt, M., & Hedenqvist, M.S. (2010). Properties of wheat gluten/poly(lactic acid)

504   laminates.   *Journal   of   Agricultural   and   Food   Chemistry*,   *58*,   7344–7350.

505   https://doi.org/10.1021/jf1003144.

506   Cho, S. W., Gällstedt, M., Johansson, E., & Hedenqvist, M. S. (2011). Injection-molded

507   nanocomposites and materials based on wheat gluten. *International Journal of Biological

508   Macromolecules*, *48*, 146–152. https://doi.org/10.1016/j.ijbiomac.2010.10.012.

509   Coleman, N. J., & Craig, Q. M. D. (1996). Modulated temperature differential scanning calorimetry:

510   a novel approach to pharmaceutical thermal analysis. *International Journal of Pharmaceutics*, *135*,

511   13–29. https://doi.org/10.1016/0378-5173(95)04463-9.

512 Corradini, C., Alfieri, I., Cavazza, A., Lantano, C., Lorenzi, A., Zucchetto, N., & Montenero, A.

513 (2013). Antimicrobial films containing lysozyme for active packaging obtained by sol–gel technique.

514 *Journal of Food Engineering*, *119*, 580–587. https://doi.org/10.1016/j.jfoodeng.2013.05.046.

515 Couchman, P. R., & Karasz, F. E. (1978). A classical thermodynamic discussion of the effect of

516 composition on glass-transition temperatures. *Macromolecules*, *11*, 117–119.

517 https://doi.org/10.1021/ma60061a021.

518 Das, O., Capezza, A. J., Mårtensson, J., Dong, Y., Neisiany, R. E., Pelcastre, L., Jiang, L., Xu, Q.,

519 Olsson, R. T., & Hedenqvist, M. S. (2020). The effect of carbon black on the properties of plasticised

520 wheat gluten biopolymer. *Molecules, 25*, 2279. https://doi.org/10.3390/molecules25102279.

521 Das, O., Loho, T. A., Capezza, A. J., Lemrhari, I., & Hedenqvist, M. S. (2018). A novel way of

522 adhering PET onto protein (Wheat Gluten) plastics to impart water resistance. *Coatings, 8*, 388.

523 https://doi.org/10.3390/COATINGS8110388.

524 Deshwal, G. K., Panjagari, N. R., & Alam, T. (2019). An overview of paper and paper based food

525 packaging materials: health safety and environmental concerns. *Journal of Food Science and*

526 *Technology, 56*, 4391–4403. https://doi.org/10.1007/s13197-019-03950-z.

527 Di Gioia, L., Cuq, B., & Guilbert, S. (1999). Thermal properties of corn gluten meal and its proteic

528 components. *International Journal of Biological Macromolecules*, *24*, 341–350.

529 https://doi.org/10.1016/S0141-8130(99)00048-3.

530 Fabbri, P., Singh, B., Leterrier, Y., Manson, J. A. E., Messori, M., & Pilati, F. (2006). Cohesive and

531 adhesive properties of polycaprolactone/silica hybrid coatings on poly(methyl methacrylate)

532 substrates. *Surface and Coatings Technology*, *200*, 6706–6712.

533 https://doi.org/10.1016/j.surfcoat.2005.10.003.

534 Farrell, A. E., Plevin, R. J., Turner, B. T., Jones, A. D., O'Hare, M., & Kammen, D. M. (2006).

535 Ethanol can contribute to energy and environmental goals. *Science*, *311*, 506–508.

536 https://doi.org/10.1126/science.1121416.

537 Farris, S., Introzzi, L., Biagioni, P., Holz, T., Schiraldi, A., & Piergiovanni, L. (2011). Wetting of

538 biopolymer coatings: contact angle kinetics and image analysis investigation. *Langmuir, 27*, 7563–

539 7574. https://doi.org/10.1021/la2017006.

540 Farris, S., Introzzi, L., Fuentes-Alventosa, J. M., Santo, N., Rocca, R., & Piergiovanni, L. (2012).

541 Self-assembled pullulan-silica oxygen barrier hybrid coatings for food packaging applications.

542 *Journal of Agricultural and Food Chemistry*, *60*, 782–790. https://doi.org/10.1021/jf204033d.

543 Fuentes-Alventosa, J. M., Introzzi, L., Santo, N., Cerri, G., Brundu, A., Farris, S. (2013). Self-

544 assembled nanostructured biohybrid coatings by an integrated 'sol-gel – intercalation' approach. *RSC*

545 *Advances*, *3*, 25086–25096. https://doi.org/10.1039/C3RA45640D.

546 Gällstedt, M., Brottman, A., & Hedenqvist, M. S. (2005). Packaging-related properties of protein-

547 and chitosan-coated paper. *Packaging Technology and Science, 18*, 16–170.

548 https://doi.org/10.1002/pts.685.

549 Gatto, M., Ochi, D., Pedroso Yoshida, C. M., & Ferreira da Silva, C. (2019). Study of chitosan with

550 different degrees of acetylation as cardboard paper coating. *Carbohydrate Polymers*, *210*, 56–63.

551 https://doi.org/10.1016/j.carbpol.2019.01.053.

552 Gennadios, A., Brandenburg, A. H., Park, J. W., Weller, C. L., & Testin, R. F. (1994). Water vapor

553 permeability of wheat gluten and soy protein isolate films. *Industrial Crops and Products*, *2*, 189–

554 195. https://doi.org/10.1016/0926-6690(94)90035-3.

555 Gontard, N., Guilbert, S., & Cuq, J. L. (1992). Edible wheat gluten films: Influence of the main

556 process variables on film properties using response-surface methodology. *Journal of Food Science*,

557 *57*, 190–195. https://doi.org/10.1111/j.1365-2621.1992.tb05453.x.

558 Gontard, N., Thibault, R., Cuq, B., & Guilbert, S. (1996). Influence of relative humidity and film

559 composition on oxygen and carbon dioxide permeabilities of edible films. *Journal of Agricultural*

560 *and Food Chemistry*, *44*, 1064–1069. https://doi.org/10.1021/jf9504327.

561 Guillaume, C., Pinte, J., Gontard, N., & Gastaldi, E. (2010). Wheat gluten-coated papers for bio-

562 based food packaging: structure, surface and transfer properties. *Food Research International*, *43*,

563 1395–1401. https://doi.org/10.1016/j.foodres.2010.04.014.

564 Hatakeyama, T., & Quinn, F. X. (1999). Thermal Analysis: Fundamentals and Applications to

565 Polymer Science (2nd ed.). New York: John Wiley and Sons.

566 Hedenqvist, M. S. (2018). Barrier packaging materials. In M. Kutz (Ed.), *Handbook of Environmental*

567 *Degradation of Materials* (pp. 559-581). Amsterdam: Elsevier, Inc.

568 Jones, P., & Comfort, D. (2017). The forest, paper and packaging industry and sustainability.

569 *International Journal of Sales, Retailing and Marketing, 6*, 3–21.

570 Kalichevsky, M. T., Jaroskiewicz, E. M., & Blanshard, J. M. V. (1992). Glass transition of gluten. 1:

571 Gluten and gluten-sugar mixtures. *International Journal of Biological Macromolecules*, *14*, 257–266.

572 https://doi.org/10.1016/S0141-8130(05)80038-8.

573 Karbowiak, T., Debeaufort, F., & Voilley, A. (2006). Importance of surface tension characterization

574 for food, pharmaceutical and packaging products: a review. *Critical Reviews in Food Science and*

575 *Nutrition, 46*, 391–407. https://doi.org/10.1080/10408390591000884.

576 Kim, S. W. (2008). Preparation and barrier property of poly(vinyl alcohol)/SiO2 hybrid coating films.

577 *Korean Journal of Chemical Engineering*, *25*, 1195–1200. https://doi.org/10.1007/s11814-008-0197-

578 9.

579 Krimm, S., & Bandekar, J. (1986). Vibrational spectroscopy and conformation of peptides,

580 polypeptides, and proteins. *Advances in Protein Chemistry*, *38*, 181–364.

581 https://doi.org/10.1016/S0065-3233(08)60528-8.

582 Krook, M., & Hedenqvist, M. S. (2002). Polymer–clay nanocomposites, one way to improve the

583 barrier properties of polymers used in packaging. In: Conference proceedings from the Tappi place

584 conf.

585 Lantano, C., Alfieri, I., Cavazza, A., Corradini, C., Lorenzi, A., Zucchetto, N., & Montenero, A.

586 (2014). Natamycin based sol–gel antimicrobial coatings on polylactic acid films for food packaging.

587 *Food Chemistry*, *165*, 342–347. https://doi.org/10.1016/j.foodchem.2014.05.066

588 Lee, S. Y., Lee, J. D., & Yang, S. M. (1999). Preparation of silica-based hybrid materials coated on

589 polypropylene   film.   *Journal   of   Materials   Science*,   *34*,   1233–1241.

590 https://doi.org/10.1023/A:1004517208507.

591 Lein, H. L. Coatings and surfaces with hydrophobic and anti-icing properties. In M. Benelmekki, &

592 A. Erbe (Eds.), *Nanostructured Thin Films* (pp. 257-269). Amsterdam: Elsevier, Inc.

593 Lens, J. P., de Graaf, L. A., Stevels, W. M., Dietz, C. H. J. T., Verhelst, K. C. S., Vereijken, J. M., &

594 Kolster, P. (2003). Influence of processing and storage conditions on the mechanical and barrier

595 properties of films cast from aqueous wheat gluten dispersions. *Industrial Crops and Products*, *17*,

596 119–130. https://doi.org/10.1016/S0926-6690(02)00092-4.

597 Liu, X., Chen, K., Wang, J., Wang, Y., Tang, Y., Gao, X., Zhu, L., Li, X., & Li, J. (2020). An on-

598 package colorimetric sensing label based on a sol-gel matrix for fish freshness monitoring. *Food

599 Chemistry*, *307*, 125580. https://doi.org/10.1016/j.foodchem.2019.125580.

600 Mascheroni, E., Guillard, V., Gastaldi, E., Gontard, N., & Chalier, P. (2011). Anti-microbial

601 effectiveness of relative humidity-controlled carvacrol release from wheat gluten/montmorillonite

602 coated papers. *Food Control*, *22*, 1582–1591. https://doi.org/10.1016/j.foodcont.2011.03.014.

603 Mazhari Mousavi, S. M., Afra, E., Tajvidi, M., Bousfiled, D.W., & Dehghani-Firouzabadi, M. (2017).

604 Cellulose nanofiber/carboxymethyl cellulose blends as an efficient coating to improve the structure

605 and barrier properties of paperboard. *Cellulose*, *24*, 3001–3014. https://doi.org/10.1007/s10570-017-

606 1299-5.

607 Menzel, C., & Koch, K. (2014). Impact of the coating process on the molecular structure of starch-

608 based barrier coatings. *Journal of Applied Polymer Science*, *131*, 1–9.

609 https://doi.org/10.1002/app.41190.

610 Minelli, M., De Angelis, M. G., Doghieri, F., Rocchetti, M., & Montenero, A. (2010). Barrier

611 properties of organic-inorganic hybrid coatings based on polyvinyl alcohol with improved water

612 resistance. *Polymer Engineering & Science*, *50*, 144–153. https://doi.org/10.1002/pen.21440.

613 Mir, S. A., Wani, H. M., Wani, I. A., Singh, P., & Wani, A. A. (2017). Testing of paper as packaging

614 material for food industry. In P. Singh, A. A. Wani, & H. C. Langowski (Eds.) *Food packaging*

615 *materials-testing and quality assurance* (ch. 8). Boca Raton: CRC Press.

616 Mirmehdi, S., Gherardi Hein, P. R., Grígoli de Luca Sarantópoulos, C. I., Dias, M. V., & Denzin

617 Tonoli, G. H. (2018). Cellulose nanofibrils/nanoclay hybrid composite as a paper coating: Effect of

618 spray time, nanoclay content and corona discharge on barrier and mechanical properties of the coated

619 papers. *Food Packaging and Shelf Life, 15*, 87–94. https://doi.org/10.1016/j.fpsl.2017.11.007.

620 Mujica Paz, H., & Gontard, N. (1997). Oxygen and carbon dioxide permeability of wheat gluten film:

621 Effect of relative humidity and temperature. *Journal of Agricultural and Food Chemistry*, *45*, 4101–

622 4105. https://doi.org/10.1021/jf970201v.

623 Mujica Paz, H., Guillard, V., Reynes, M., & Gontard, N. (2005). Ethylene permeability of wheat

624 gluten film as a function of temperature and relative humidity. *Journal of Membrane Science*, *256*,

625 108–115. https://doi.org/10.1016/j.memsci.2005.02.011.

626 Olabarrieta, I., Cho, S. W., Gällstedt, M., Sarasua, J. R., Johansson, E., & Hedenqvist, M. (2006).

627 Aging prperties of films of plasticized vital wheat gluten cast from acidic and basic solutions.

628 *Biomacromolecules*, *7*, 1657–1664. https://doi.org/10.1021/bm0600973.

629 Ottesen, V., Kumar, V., Toivakka, M., Chinga-Carrasco, G., Syverud, K., Gregersen, Ø. W. (2017).

630 Viability and properties of roll-to-roll coating of cellulose nanofibrils on recycled paperboard. *Nordic*

631 *Pulp & Paper Research Journal, 32*, 179–188. https://doi.org/10.3183/npprj-2017-32-02-p179-188

632 Parris, N., Dickey, L.C., Wiles, J.L., Moreau, R.A., & Cooke, P.H. (2000). Enzymatic hydrolysis,

633 grease permeation and water barrier properties of zein isolate coated paper. *Journal of Agricultural*

634 *and Food Chemistry*, *48*, 890–894. https://doi.org/10.1021/jf991079y

635 Razavi, R., Tajik, H., Moradi, M., Molaei, R. & Ezati, P. (2020). Antimicrobial, microscopic and

636 spectroscopic properties of cellulose paper coated with chitosan sol-gel solution formulated by

637 epsilon-poly-l-lysine and its application in active food packaging. *Carbohydrate Research*, *489*,

638 107912. https://doi.org/10.1016/j.carres.2020.107912.

639 Reis, A.B., Yoshida, C.M.P., Reis, Ana Paula C, & Franco, T.T. (2011). Application of chitosan

640 emulsion as a coating on Kraft paper. *Polymer International*, *60*, 963–969.

641 https://doi.org/10.1002/pi.3023

642 Rhim, J.W., Lee, J.-H., & Hong, S.-I. (2007). Increase in water resistance of paperboard by coating

643 with poly(lactide). *Packaging Technology and Science*, *20*, 393–402. https://doi.org/10.1002/pts.767.

644 Rosario, R., Gust, D., Garcia, A. A., Hayes, M., Taraci, J. L., Clement, T., Dailey, J. W., & Picraux,

645 S. T. (2004). Lotus effect amplifies light-induced contact angle switching. *The Journal of Physical*

646 *Chemistry B*, *108*, 12640–12642. https://doi.org/10.1021/jp0473568.

647 Rovera, C., Ghaani, M., & Farris, S. (2020). Nano-inspired oxygen barrier coatings for food

648 packaging applications: an overview. *Trends in Food Science & Technology*, *97*, 210-220.

649 https://doi.org/10.1016/j.tifs.2020.01.024.

650 Sartori, T., Feltre, G., do Amaral Sobral, P. J., Lopes da Cunha, R., & Mengalli, F. C. (2018).

651 Properties of films produced from blends of pectin and gluten. *Food Packaging and Shelf Life, 18*,

652 221–229. https://doi.org/10.1016/j.fpsl.2018.11.007.

653   Schubert, U. (2015). Chemistry and Fundamentals of the Sol-Gel Process. In D. Levy, & M. Zayat

654   (Eds.), *The Sol-Gel Handbook* (pp. 3-27). Weinheim: Wiley-VCH Verlag GmbH & Co. KGaA.

655   Startek, K., Marczak, J., & Lukowiak, A. (2020). Oxygen barrier enhancement of polymeric foil by

656   sol-gel-derived   hybrid   silica   layers.   *Polymers*,   *195*,   122437.

657   https://doi.org/10.1016/j.polymer.2020.122437.

658   Störmer, A., Bott, J., Kemmer, D., & Franz, R. (2017). Critical review of the migration potential of

659   nanoparticles in food contact plastics. *Trends in Food Science & Technology, 63*, 39–50.

660   https://doi.org/10.1016/j.tifs.2017.01.011

661   Sun, Q., Schork, F. J., & Deng, Y. (2007). Water-based polymer/clay nanocomposite suspension for

662   improving water and moisture barrier in coating. *Composites Science & Technology, 67,* 1823–1829.

663   https://doi.org/10.1016/j.compscitech.2006.10.022.

664   Tong, Q., Xiao, Q., & Lim, L. T. (2008). Preparation and properties of pullulan–alginate–

665   carboxymethylcellulose   blend   films.   *Food   Research   International*,   *41*,   1007–1014.

666   https://doi.org/10.1016/j.foodres.2008.08.005.

667   Tunc, S., Angellier, H., Cahyana, Y., Chalier, P., Gontard, N., & Gastaldi, E. (2007). Functional

668   properties of wheat gluten/montmorillonite nanocomposite films processed by casting. *Journal of

669   Membrane Science*, *289*, 159–168. https://doi.org/10.1016/j.memsci.2006.11.050.

670   Türe, H., Gällstedt, M., Johansson, E., & Hedenqvist, M. S. (2013). Wheat-gluten/montmorillonite

671   clay multilayer-coated paperboards with high barrier properties. *Industrial Crops and Produtcs, 51*,

672   1–6. https://doi.org/10.1016/j.indcrop.2013.08.054.

673   Türe, H., Blomfeldt, T. O. J., Gällstedt, M., Hedenqvist, M. S., & Farris, S. (2013). Nanostructured

674   silica/wheat gluten hybrid materials prepared by catalytic sol-gel chemistry. *Macromolecular

675   Chemistry and Physics*, *214*, 1131–1139. https://doi.org/10.1002/macp.201200646.

676 Uragami, T., Okazaki, K., Matsugi, H., & Miyata, T. (2002). Structure and permeation characteristics

677 of an aqueous ethanol solution of organic-inorganic hybrid membranes composed of poly(vinyl

678 alcohol) and tetraethoxysilane. *Macromolecules*, *35*, 9156–9163.

679 https://doi.org/10.1021/ma020850u.

680 Wu, Q., Andersson, R. L., Holgate, T., Johansson, E., Gedde, U. W., Olsson, R. T., & Hedenqvist,

681 M. S. (2014). Highly porous flame-retardant and sustainable biofoams based on wheat gluten and in

682 situ polymerized silica. *Journal of Materials Chemistry A*, *2*, 20996-21009.

683 https://doi.org/10.1039/c4ta04787g.

684 Wu, X., Zheng, L., & Wu, D. (2005). Fabrication of superhydrophobic surfaces from microstructured

685 ZnO-based surfaces via a wet-chemical route. *Langmuir*, *21*, 2665–2667.

686 https://doi.org/10.1021/la050275y.

687 Zhang, W., Xiao, H., & Qian, L. (2014). Enhanced water vapour barrier and grease resistance of paper

688 bilayer-coated with chitosan and beeswax. *Carbohydrate Polymers*, *101*, 401–406.

689 https://doi.org/10.1016/j.carbpol.2013.09.097.

690

691

692 **Captions to Illustrations**

693

694 **Figure 1.** Schematic representation of the hydrolysis (a) and condensation (b) reactions; and the

695 hybrid network formation between an exemplificative 5-amino acids sequence (Ser-Arg-Thr-Asp-

696 Glu) of the WG protein and the silica network.

697

698 **Figure 2.** Representative cross-section scanning electron microscopy image (400×) of a

699 paperboard-hybrid coating composite produced in this work.

700

701 **Figure 3.** FTIR-ATR spectra of hybrid coatings within 3850 cm^{-1} ÷ 2400 cm^{-1} (a), 1720 ÷ 1470 cm^{-1}

702 (b), and 1150 cm^{-1} ÷ 700 cm^{-1} (c) spectral ranges. Symbols: (━) pure WG; (━) reacted TEOS; (━

703) H$_3$; (━) H$_2$; (━) H$_1$; (━) H$_{0.75}$; (━) H$_{0.5}$.

704

705 **Figure 4.** First heating (a) and second heating (b) DSC traces of the pure WG (H$_0$) and the hybrid (H$_1$

706 and H$_{0.5}$) materials.

707

708 **Figure 5.** Specific heat capacity (c_p) profile of pure WG and hybrid materials H$_1$ and H$_{0.5}$ within the

709 temperature range 300 K–450 K (27 °C–177 °C).

710

711 **Figure 6.** SEM images of uncoated (a), WG-coated (b), and hybrid (H$_3$, H$_1$, H$_{0.5}$)-coated (c-f)

712 paperboard samples (see the text for details).

713

714 **Figure 7.** Water vapor transmission rate (WVTR) measured for the neat paperboard, paperboard

715 coated with gluten (H$_0$), and paperboard coated with the hybrid formulations (H$_3$ − H$_{0.5}$) at 23°C and

716 65% RH.

717 **Tables**

718

719 **Table 1**

720 Formulation parameters of the WG-based coatings used in this work.

721

Exp. n°	Code Name	WG (wt-%)	$Si(OH)_4$ (wt-%)	(O/I*) ratio
1	Neat paperboard	0	0	/
2	H_0	20	0	/
3	H_3	15	5	3
4	H_2	13.3	6.7	2
5	H_1	10	10	1
6	$H_{0.75}$	8.6	11.4	0.75
7	$H_{0.5}$	6.7	13.3	0.5

722

723 * "I" refers to the silanol form – $Si(OH)_4$, calculated from the initial TEOS content and assuming

724 completion of the hydrolysis reaction. Roman superscripts denote statistically significant differences

725 ($p<0.05$).

726

727

728

729

730

731

732

733

734

735

736

31

737 **Table 2**

738 Initial (θ_0) and final (θ_{60}) contact angle values for an uncoated Teflon® substrate, uncoated

739 paperboard and the six biopolymer hybrid coatings.

740

Coating formulation	θ (°) t_0	θ (°) t_{60}
Teflon®	89.4 ± 2.9^a	87.4 ± 2.6^A
Neat paperboard	125.6 ± 7.1^b	124.3 ± 6.0^B
H$_0$	70.8 ± 3.8^{cd}	61.7 ± 2.7^C *
H$_3$	78.6 ± 2.8^e	53.3 ± 1.0^D *
H$_2$	77.7 ± 2.4^e	67.6 ± 5.8^C *
H$_1$	67.1 ± 4.9^d	63.1 ± 3.5^C
H$_{0.75}$	77.5 ± 5.0^{ce}	67.5 ± 8.4^C
H$_{0.5}$	76.1 ± 6.2^{ce}	67.8 ± 9.4^C

741

742 Roman superscripts denote statistically significant differences between samples (coating

743 formulations) within the same group (t_0 and t_{60}). *Denotes statistically significant differences between

744 groups for the same sample (the difference between θ_0 and θ_{60} for each coating formulation).

Table 3. WVTR for paper-based materials coated with different biopolymers.

Biopolymer type	Paper type	Application	Coat wt (g/m^2)	WVTR $(g/(m^2 \, day))$	Ref.
rCNF 1%	Paperboard	Rod coater	1.6	450	Mazhari Mousavi *et al.*, 2017
gCNF 1%	Paperboard	Rod coater	2.6	370	Mazhari Mousavi *et al.*, 2017
rCNF 3%/CMC	Paperboard	Rod coater	6.9	400	Mazhari Mousavi *et al.*, 2017
gCNF 3%/CMC	Paperboard	Rod coater	7.8	410	Mazhari Mousavi *et al.*, 2017
PCL-2%	Offset printed paper board	K202 coater	N.D. (thickness ~ 6.1 µm)	533	Bota *et al.*, 2017
PCL-2% SiO$_2$+0.5% of Al$_2$O$_3$	Offset printed paper board	K202 coater	N.D. (thickness ~ 6.1 µm)	593	Bota *et al.*, 2017
PCL-2% SiO2+0.5% of ZnO	Offset printed paper board	K202 coater	N.D. (thickness ~ 6.1 µm).	512	Bota *et al.*, 2017
CP-2	Cardboard paper	Bar coater	252.4	281	Gatto *et al.*, 2019
CP-48	Cardboard paper	Bar coater	259.9	291	Gatto *et al.*, 2019
Zein	Kraft paper	Spray coating	10	881	Parris *et al.*, 2000
Chitosan-palmitic acid	Kraft paper	Wire bar coater	5.3	553	Reis *et al.*, 2011
Chitosan beeswax bilayer	Paper	Multicoater	3 wt%	53	Zhang *et al.*, 2014
PLA	Paperboard	Wire bar coating	~50	9.7	Rhim et al., 2007
Starch-citric acid	Paper	Bench coater and wire wound bar	15-18	16-41	Menzel & Koch, 2014

Abbrevetions: rCNF (Refiner-produced cellulose nanofiber), gCNF (grinder produced cellulose nanofiber), CMC (carboxymethyl cellulose), PCL (polycaprolactone), CP-2 (chitosan of 2% degree of acetylation), CP-2 (chitosan of 48% degree of acetylation), PLA (Poly(lactide). N.D. Not determined.

33

Supporting Information
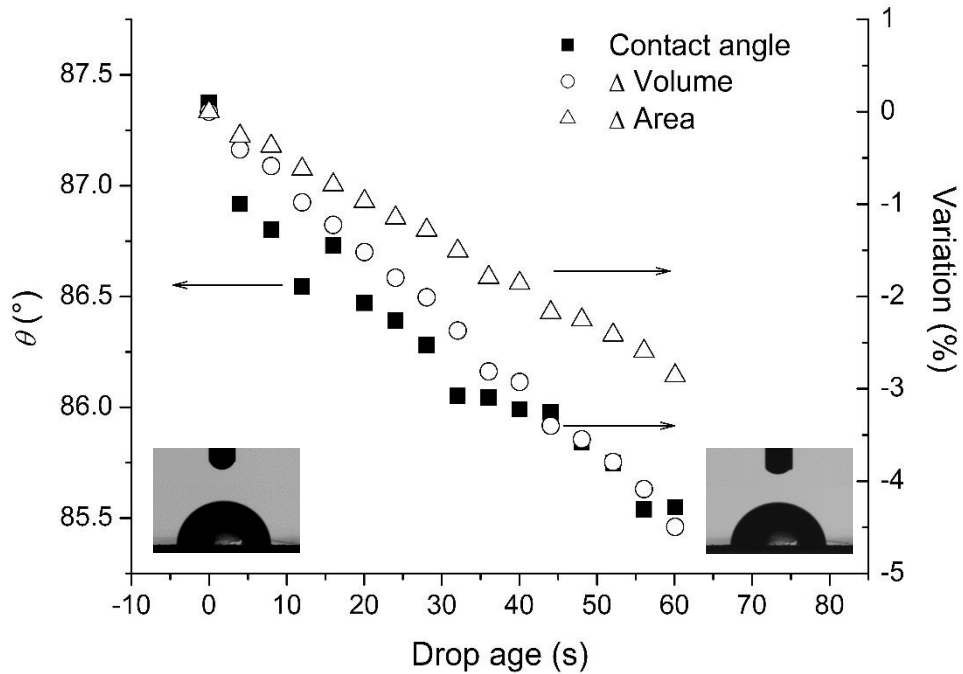
Figure S1. Contact angle, droplet volume and droplet surface area evolution during 60 s over a

Teflon® substrate for quantification of the evaporation phenomenon. The water droplet profile at t_0

(left) and t_{60} (right) is also shown.
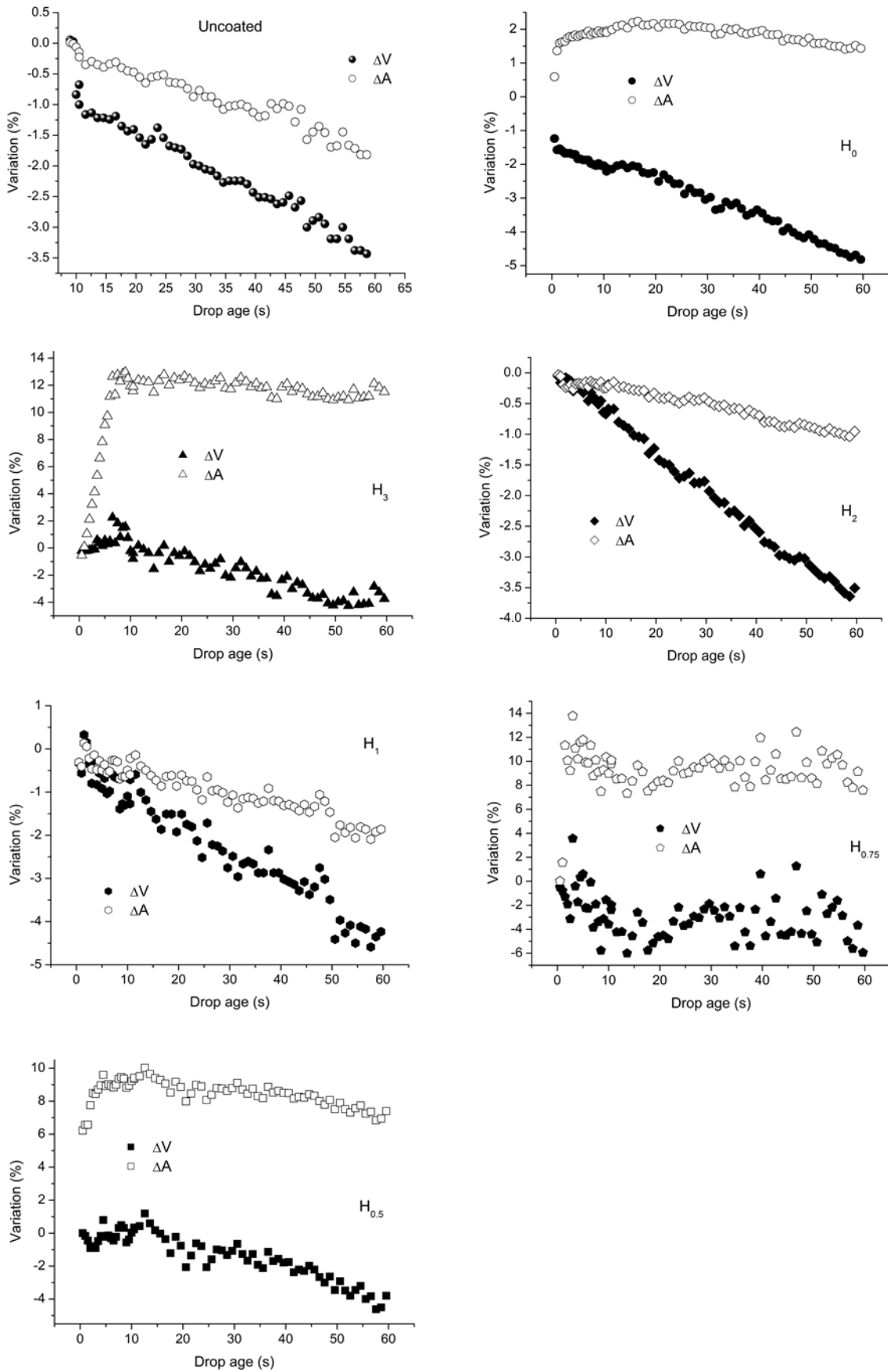
761
762
763 **Figure S2.** Representative plots displaying the droplet volume and surface area variation over a 60 s

764 time span for both uncoated and coated samples.
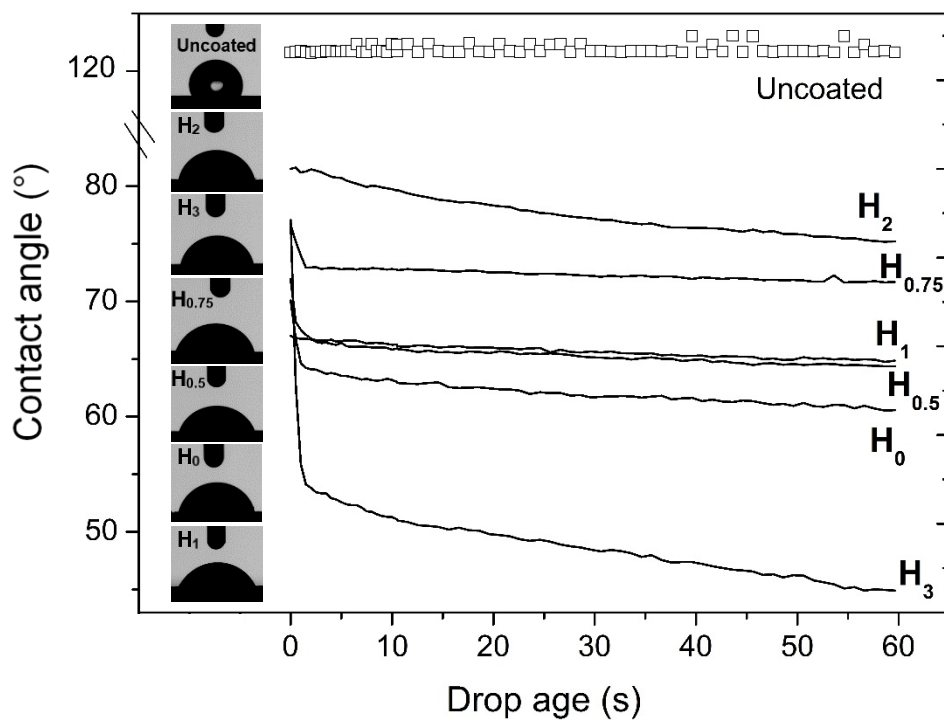
Figure S3. Water contact angle evolution during the 60 s period of analysis. The water droplet profile

at t_0 is also displayed for both uncoated and coated paperboard samples.

Figure 1
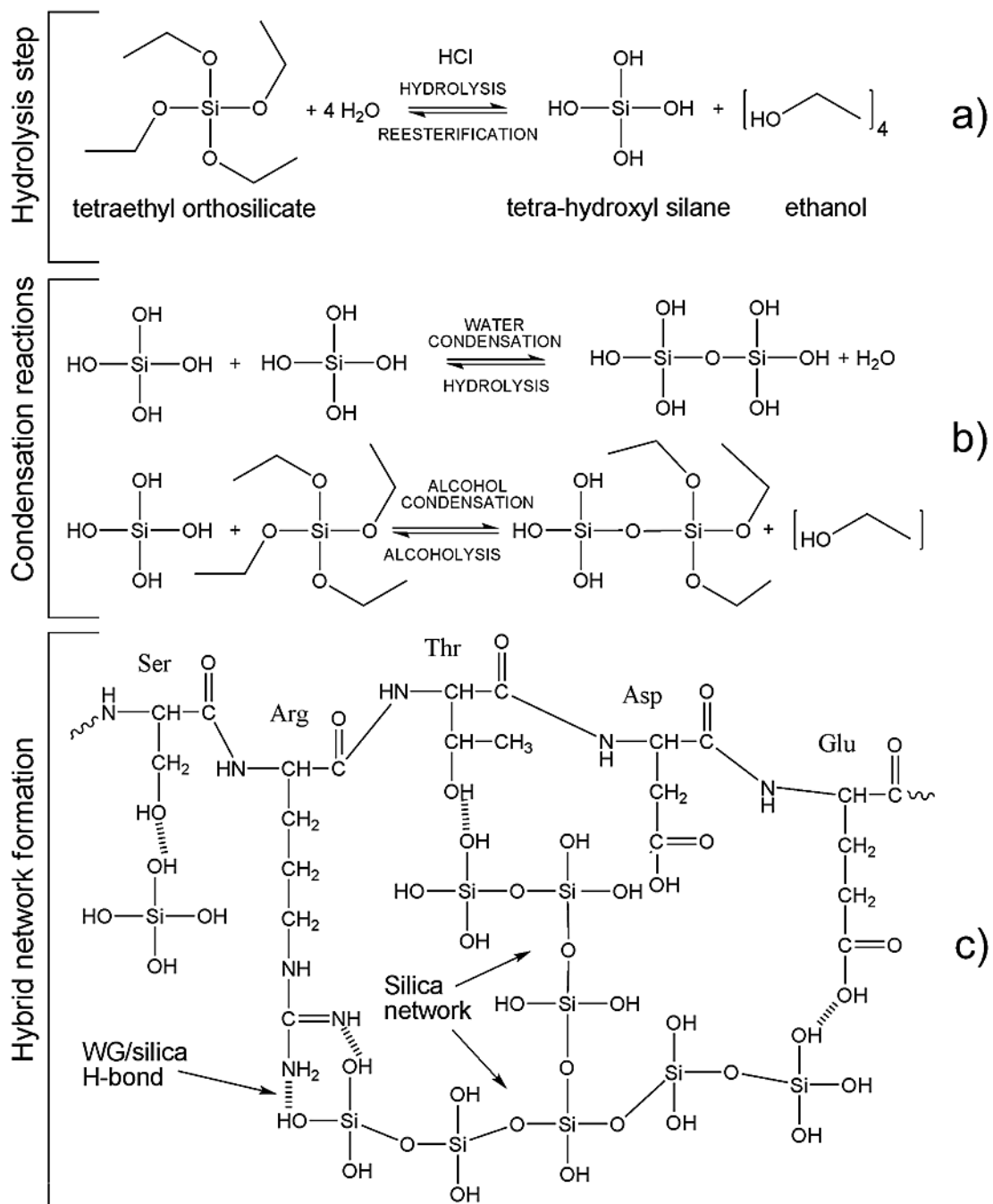
Figure 1

Figure 2
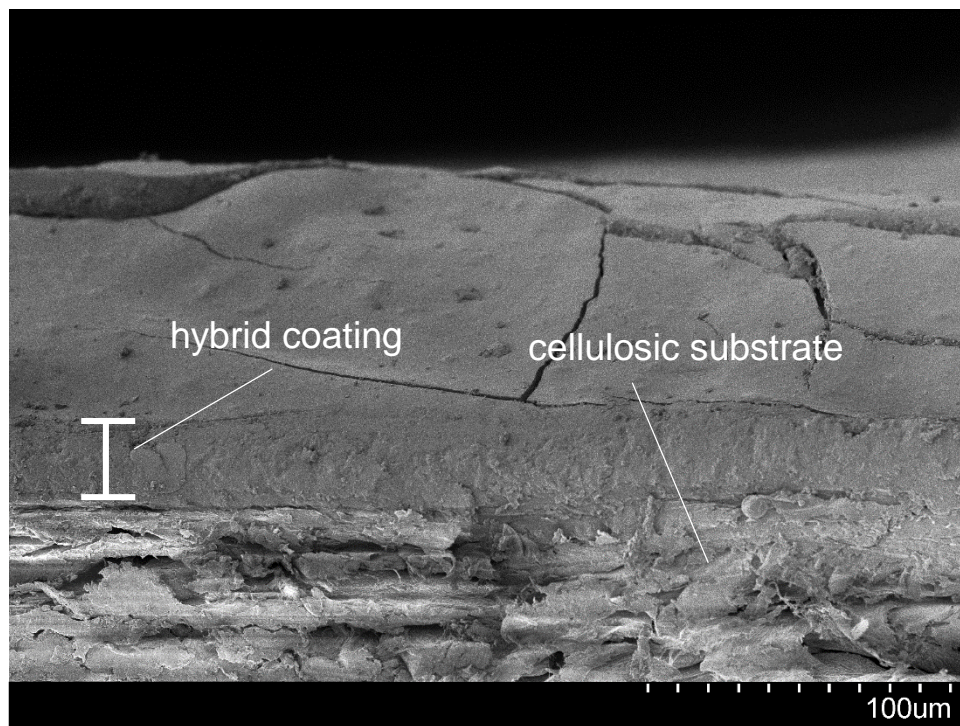
Figure 2

Figure 3
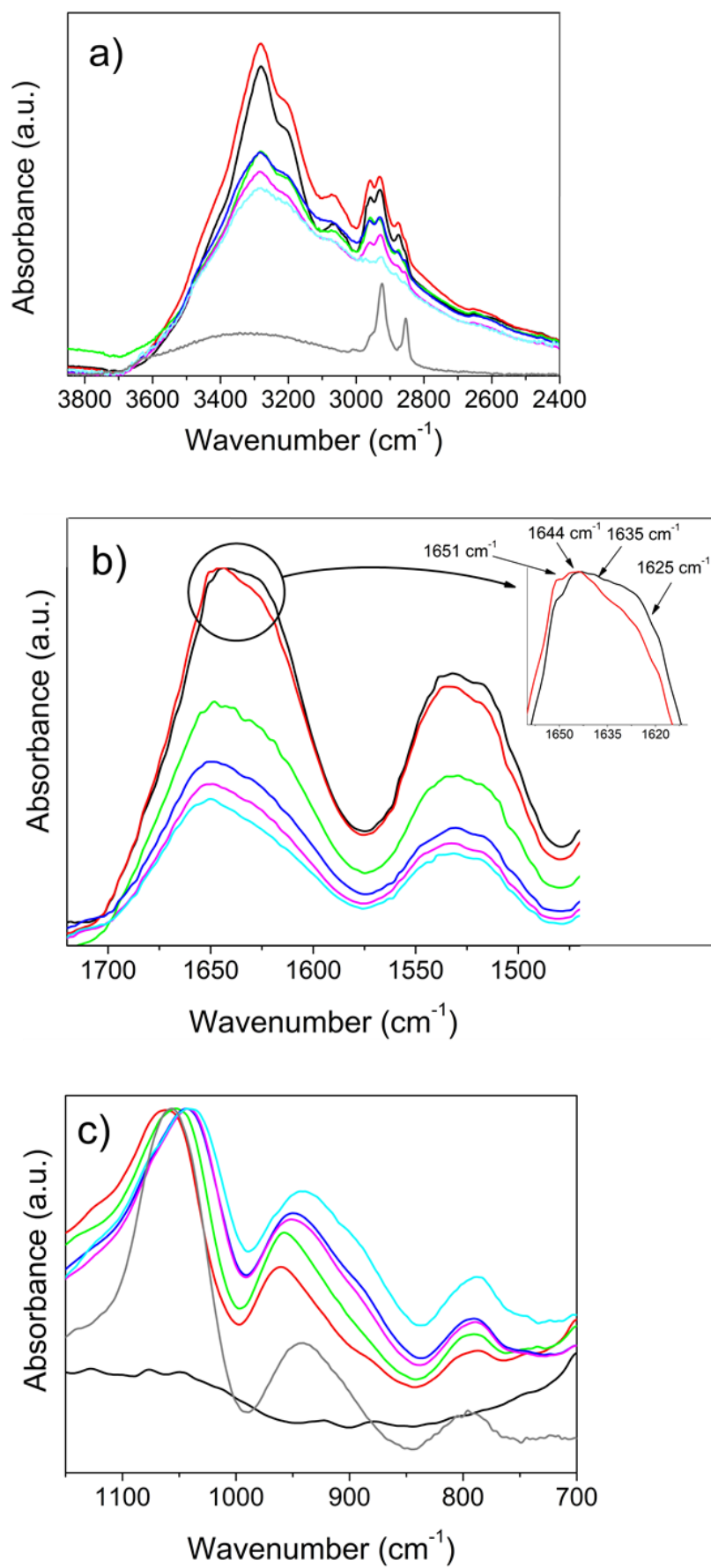
Figure 3

Figure 4
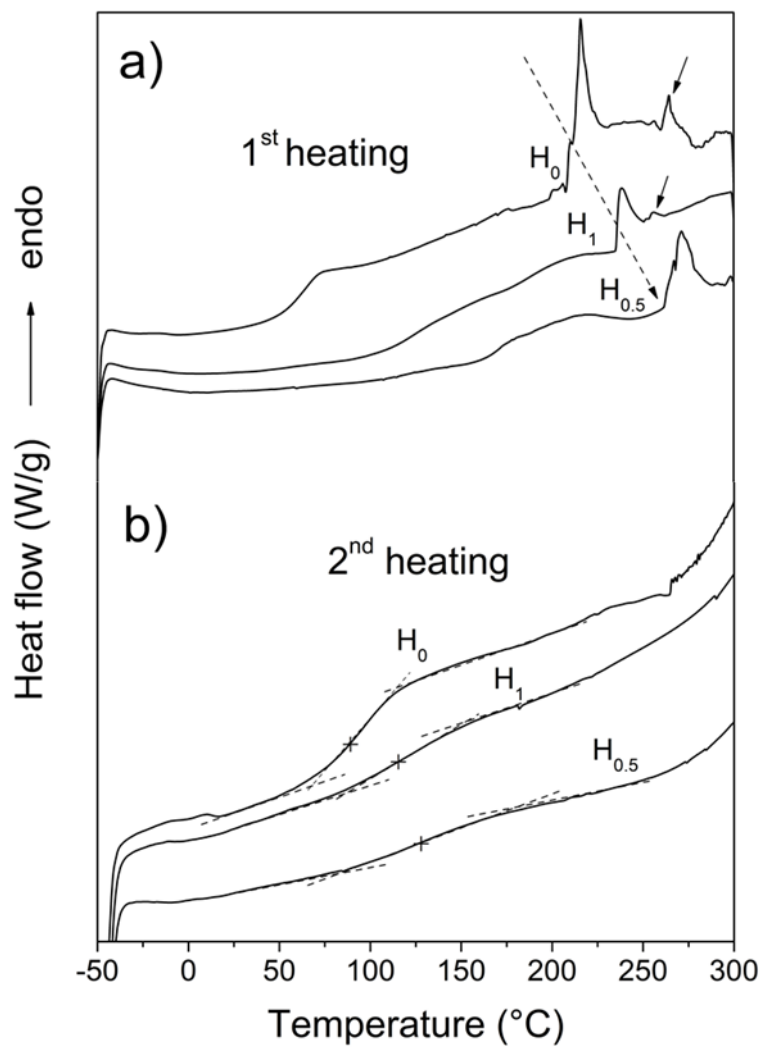
**Figure 4**

Figure 5

Figure 5
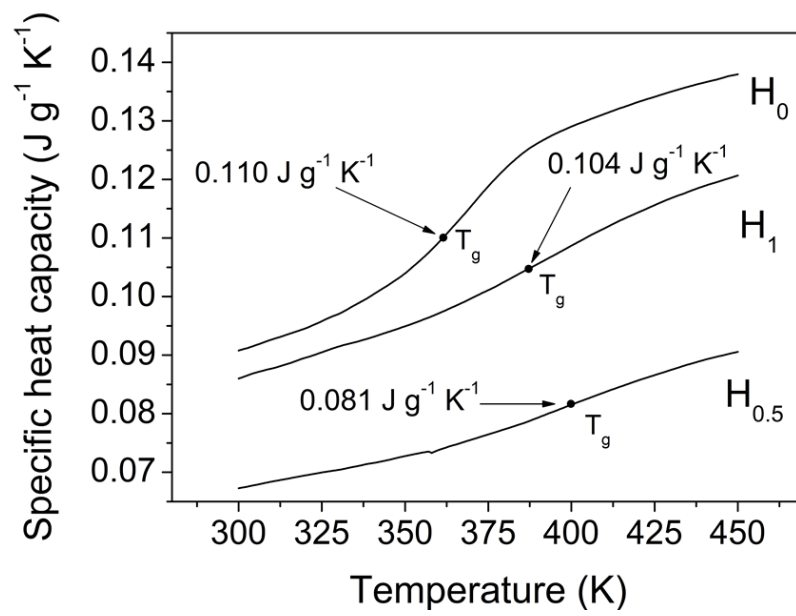
Figure 6
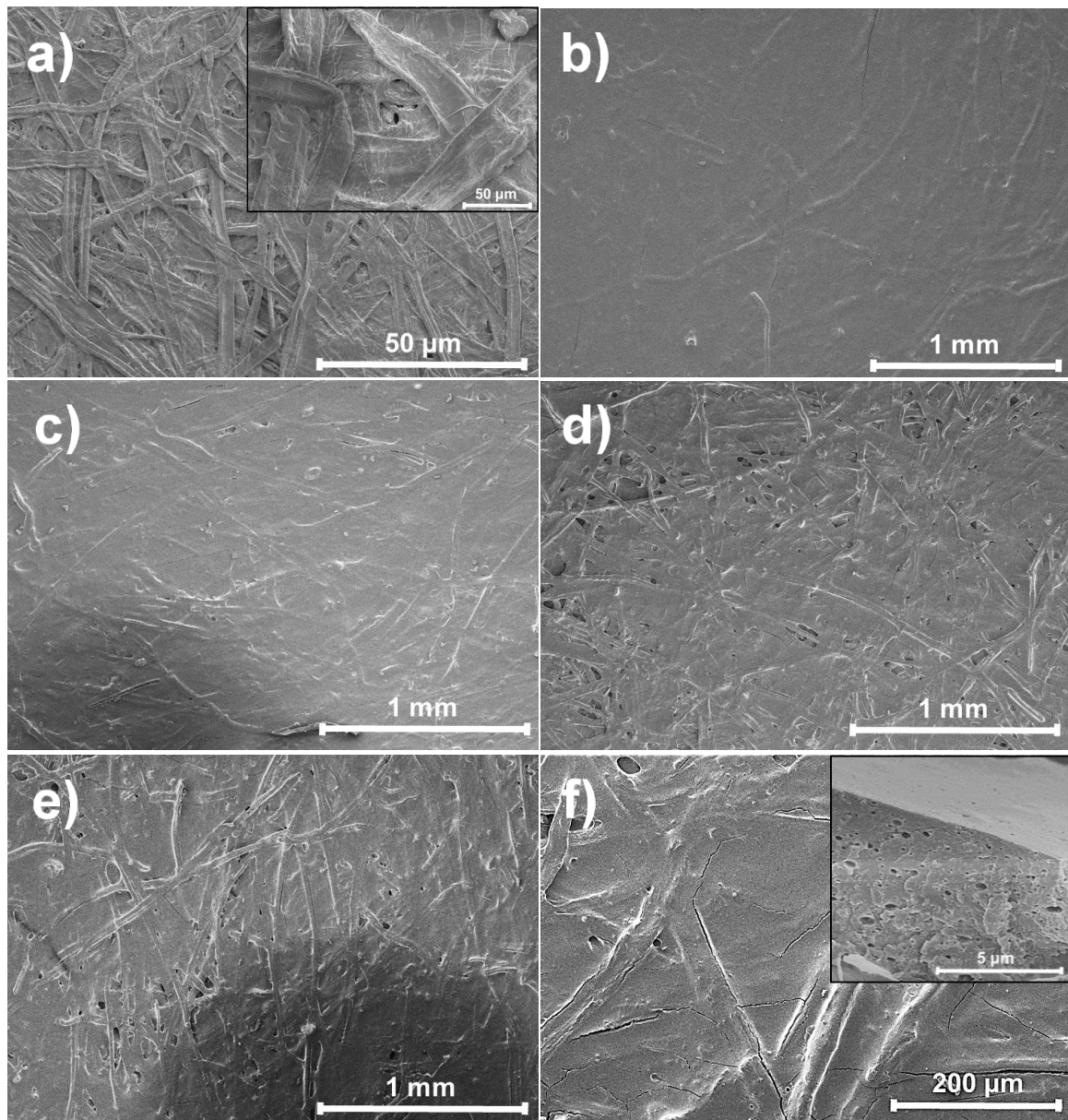
Figure 6

Figure 7

Figure 7
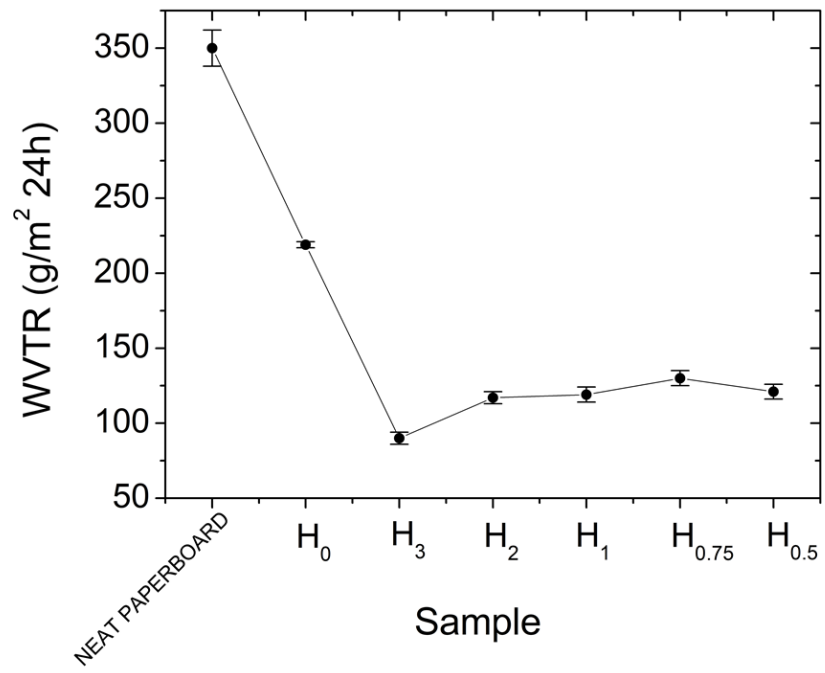
Author statement

Conceptualization: M.H. and S.F.; methodology, M.H., H.T. and S.F.; formal analysis, H.T., C.R. and S.F.; writing—original draft preparation, S. F.; writing—review and editing, M.H., H.T., C. R. and S.F.; visualization, S.F.; supervision, M. H. and S.F. All authors have read and agreed to the published version of the manuscript.